Nanoscale Research Letters

NANO EXPRESS Open Access

Fabrication of Z-scheme Ag_3PO_4/TiO_2 Heterostructures for Enhancing Visible Photocatalytic Activity

Wenhui Liu, Dengdeng Liu, Kun Wang, Xiaodan Yang, Shuangqi Hu* and Lishuang Hu*

Abstract

In this paper, a synthetical study of the composite Ag_3PO_4/TiO_2 photocatalyst, synthesized by simple two-step method, is carried out. Supplementary characterization tools such as X-ray diffraction, scanning electron microscopy, transmission electron microscopy, high-resolution transmission electron microscopy, energy dispersive X-ray spectroscopy, X-ray photoelectron spectroscopy, and UV-vis diffuse reflectance spectroscopy were adopted in this research. The outcomes showed that highly crystalline and good morphology can be observed. In the experiment of photocatalytic performance, $TiO_2$400/Ag_3PO_4 shows the best photocatalytic activity, and the photocatalytic degradation rate reached almost 100% after illuminating for 25 min. The reaction rate constant of $TiO_2$400/Ag_3PO_4 is the largest, which is 0.02286 min^{-1}, twice that of Ag_3PO_4 and 6.6 times that of the minimum value of $TiO_2$400. The degradation effect of $TiO_2$400/Ag_3PO_4 shows good stability after recycling the photocatalyst four times. Trapping experiments for the active catalytic species reveals that the main factors are holes (h^+) and superoxide anions (O·− 2), while hydroxyl radical (·OH) plays partially degradation. On this basis, a *Z*-scheme reaction mechanism of Ag_3PO_4/TiO_2 heterogeneous structure is put forward, and its degradation mechanism is expounded.

Keywords: Composite, Heterostructures, Superoxide anion, Photocatalytic degradation

Background

Semiconductor photocatalysts have attracted increasing interest due to extenstive use in organic pollutant degradation and solar cells [1–6]. As the representative of semiconductor-based photocatalysts, TiO_2 has been extensively investigated because of its excellent physical-chemical properties [7, 8]. However, the pure TiO_2 photocatalyst has certain disadvantages in practical applications such as its wide band gap (3.2 eV for anatase and 3.0 eV for rutile), which leads to poor visible response.

A silver-based compound such as Ag_2O, AgX (X = Cl, Br, I), Ag_3PO_4, Ag_2CrO_4, have been recently used for photocatalytic applications [9–12]. Among others, silver orthophosphate (Ag_3PO_4) has already attracted attention from many researchers because Ag_3PO_4 has a band gap of 2.45 eV and strong absorption at less than 520 nm. The quantum yield of Ag_3PO_4 is over 90%. It is a good visible-light photocatalyst. However, due to the formation of Ag^0 on the surface of the catalyst ($4Ag_3PO_4 + 6H_2O + 12h^+ + 12e^- \rightarrow 12Ag^0 + 4H_3PO_4 + 3O_2$) during the photocatalytic reaction, the reuse of Ag_3PO_4 is a major problem. Therefore, it is a common practice to reduce photocatalytic corrosion of Ag_3PO_4 and ensure good catalytic activity of Ag_3PO_4. Based on literature precedence, it is known that compounding can effectively improve the photocatalytic performance of both semiconductor materials. After compounding, the separation effect of photogenerated electrons and holes is strengthened, contributing to enhance the photocatalytic activity of composite materials. Numerous researchers have investigated heterojunctions such as Bi_2O_3-Bi_2WO_6, TiO_2/Bi_2WO_6, ZnO/CdSe, and Ag_3PO_4/TiO_2 [2, 13–15]. Compared with single-phase photocatalysts, heterojunction photocatalysts can expand the light response range by coupling matched electronic structure materials. And because of the synergistic effect between components, charge can be transferred through many ways to further improve heterojunction photocatalytic activity.

* Correspondence: shuangqihuzb@163.com; hlsly1314@163.com
Environmental and Safety Engineering Institute, North University of China, Taiyuan 030051, Shanxi, People's Republic of China

Based on the above analysis, Ag_3PO_4-based semiconductor composites with synergistic enhancement effect were designed to improve carrier recombination defects and Ag_3PO_4-based semiconductor composites catalytic performance. In this paper, nano-sized TiO_2 was prepared by solvothermal method, and then the nanoparticles of $TiO_2$400 were deposited on the surface of Ag_3PO_4 at room temperature to obtain TiO_2/Ag_3PO_4 composites. The photocatalytic activity of TiO_2/Ag_3PO_4 composite was tested using RhB dye (rhodamine B).

Methods

Hydrothermal Preparation of Nano-sized TiO_2

0.4 g P123 was added to a mixed solution containing 7.6 mL absolute ethanol and 0.5 mL deionized water and stirred until P123 was completely dissolved. The clarified solution was labeled as A solution. Then a mixed solution containing 2.5 mL butyl titanate (TBOT) and 1.4 mL concentrated hydrochloric acid (12 mol/L) was prepared and labeled as B solution. The solution B was added to solution A by drop. After stirring for 30 min, 32 mL ethylene glycol (EG) was added to the solution and stirred for 30 min. Then, the solution was placed in oven, at 140 °C, high temperature, and high pressure for 24 h. Natural cooling, centrifugal washing, separation, collection of sediments, and drying at 80 °C oven for 8 h. The white precipitation was calcined in muffle furnace at different temperatures (300 °C, 400 °C, 500 °C) and marked as standby of $TiO_2$300, $TiO_2$400, and $TiO_2$500, respectively.

Preparation of TiO_2/Ag_3PO_4 Photocatalyst

The 0.1 g TiO_2 powder was added to the 30-mL silver nitrate solution containing 0.612 g $AgNO_3$ and then treated by ultrasound for 30 min to make TiO_2 dispersed uniformly. We added 30-mL solution containing 0.43 g $Na_2HPO_4.12H_2O$ and stirred for 120 min at ambient temperature. By centrifugation, cleaning with deionized water and anhydrous ethanol, the precipitates were separated, collected, and dried at 60 °C. The products were named as $TiO_2$300/Ag_3PO_4, $TiO_2$400/Ag_3PO_4, and $TiO_2$500/Ag_3PO_4, respectively. Ag_3PO_4 was prepared without adding TiO_2 under the same conditions as the above process.

Characterization

The X-ray diffraction (XRD) patterns of the resulted samples were performed on a D/MaxRB X-ray diffractometer (Japan), which has a 35 kV Cu-Ka with a scanning rate of 0.02° s^{-1}, ranging from 10 to 80°. Scanning electron microscopy (SEM), JEOL, JSM-6510, and JSM-2100 transmission electron microscopy (TEM) assembly with energy dispersive X-ray spectroscopy (EDX) were used to study its morphology at 10-kV acceleration voltage. X-ray photoelectron spectroscopy (XPS) information were collected by using an ESCALAB 250 electron spectrometer under 300-W Cu Kα radiation. The basic pressure was about 3×10^{-9} mbar, Combine to refer to the C1s line at amorphous carbon 284.6 eV.

Photocatalytic Activity Measure

The photocatalytic performance of TiO_2/Ag_3PO_4 catalysts was tested by using the photodegradation of RhB in aqueous solution as the research object. Fifty milligrams of the photocatalyst was mixed with 50 mL of RhB aqueous solution (10 mg L^{-1}) and stirred in darkness for a certain time before illumination to ensure adsorption balance. In the reaction process, cooling water is used to keep the system temperature constant at room temperature. A 1000-W Xenon lamp provides illumination to simulate visible light. LAMBDA35 UV/Vis spectrophotometer was used to characterize the concentration (C) change of RhB solution at λ = 553 nm. The decolorization rate is indicated as a function of time vs C_t/C_0. Where C_0 is the concentration before illumination, and C_t is the concentration after illumination. Used catalysts were recollected to detect the cycle stability of the catalysts. The experiment was repeated four times.

Results and Discussion

XRD analysis is used to determine the phase structure and crystalline type of catalyst. The XRD spectra of the prepared catalysts were shown in Fig. 1, including $TiO_2$400, Ag_3PO_4, TiO_2/Ag_3PO_4, $TiO_2$300/Ag_3PO_4, $TiO_2$400/Ag_3PO_4, and $TiO_2$500/Ag_3PO_4. It can be obtained from the figure that the crystal structure of $TiO_2$400 is anatase (JCPDS No. 71-1166). In the XRD spectra of Ag_3PO_4, the diffraction peaks located at 20.9°,

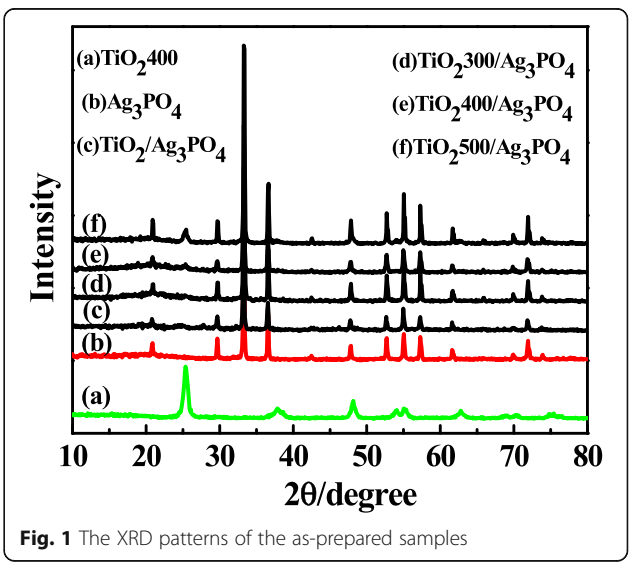

Fig. 1 The XRD patterns of the as-prepared samples

29.7°, 33.3°, 36.6°, 47.9°, 52.7°, 55.1°, 57.4°, 61.7°, and 72.0° belong to the characteristic peaks of (110), (200), (210), (211), (310), (222), (320), (321), (400), and (421) planes of Ag_3PO_4 (JCPDS No. 70-0702), respectively. The synthesized composite photocatalysts showed characteristic peaks consistent with TiO_2 and Ag_3PO_4, and the characteristic peaks of TiO_2 were 25.3° at the composite TiO_2, TiO_2300/Ag_3PO_4, TiO_2400/Ag_3PO_4, TiO_2500/Ag_3PO_4, which was consistent with the calcination temperature of TiO_2 rise, the crystallinity of TiO_2 becomes higher.

Figure 2 shows the SEM, TEM, and EDX diagrams of the catalysts of TiO_2400, Ag_3PO_4, and TiO_2400/Ag_3PO_4. Figure 2a is the spherical nanostructure TiO_2400 prepared by solvothermal method with a diameter ranging from 100 to 300 nm. Figure 2b is the Ag_3PO_4 crystal with a regular hexahedral structure. Its particle size ranges from 0.1 to 1.5 μm and has a fairly smooth surface. Figure 2c is the SEM image of the composite TiO_2400/Ag_3PO_4. It can be seen that the nanoparticles of TiO_2400 are deposited on the surface of Ag_3PO_4. The morphology of TiO_2400/Ag_3PO_4 was further explored with TEM and the TEM diagram of TiO_2400/Ag_3PO_4 is displayed in Fig. 2d. It can be observed that 200-nm nano-sized TiO_2 particles adhere to the surface of Ag_3PO_4. Figure 2e is the HRTEM of TiO_2400/Ag_3PO_4. It can be founded that TiO_2 particles are closely bound to Ag_3PO_4, and the lattice spacing of TiO_2400 and Ag_3PO_4 are 0.3516 and 0.245 nm, respectively, corresponding to (101) and (211) surfaces of TiO_2 and Ag_3PO_4. Figure 2f is the EDX diagram of TiO_2400/Ag_3PO_4. It can be seen that the sample consists of four elements: Ti, O, Ag, and P. The obvious diffraction peak of copper element is

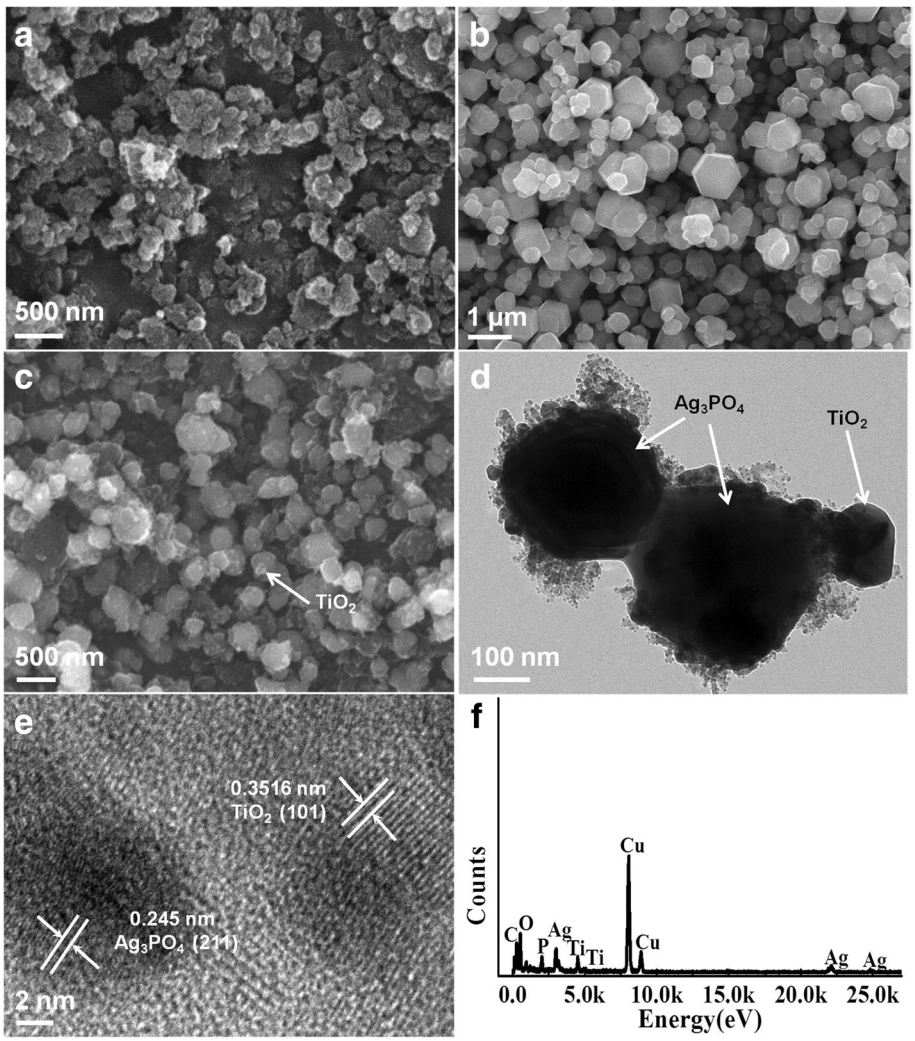

Fig. 2 SEM images of prepared photocatalysts: **a** TiO_2400, **b** Ag_3PO_4, **c** TiO_2400/Ag_3PO_4, **d** TEM image of TiO_2400/Ag_3PO_4, **e** HRTEM image of TiO_2400/Ag_3PO_4, and **f** corresponding EDX pattern of TiO_2400/Ag_3PO_4

produced by the EDX excitation source, Cu Ka. EDX confirmed the corresponding chemical elements of $TiO_2$400/Ag_3PO_4. In conclusion, it can be clearly judged that TiO_2 is loaded on the surface of Ag_3PO_4 crystals in granular form and has a good hexahedron morphology.

The product X-ray photoelectron spectroscopy (XPS) is investigated in Fig. 3. Figure 3a is the survey XPS spectrum of the product. Ti, O, Ag, P, and C five elements can be observed in the graph, of which C is the base, implying that composite coexisted with TiO_2 and Ag_3PO_4. Figure 3b is the high-resolution spectrum of Ag 3d. The two main peaks centered at binding energy 366.26 eV and 372.29 eV, assigning to Ag 3d5/2 and Ag 3d3/2, respectively. It shows that Ag is mainly Ag^+ in the photocatalyst of $TiO_2$400/Ag_3PO_4 [16]. Figure 3c shows the XPS peak of P 2p, which corresponds to P^{5+} in the PO_4^{3+} structure at 131.62 eV. Two peaks located at 457.43 eV and 464.58 eV can be attributed to Ti 2p3/2 and Ti 2p1/2 in the XPS spectrum of Ti 2p orbital (Fig. 3d). Figure 3e is the XPS of O 1s. The whole peak can be divided into three characteristic peaks, 528.9 eV, 530.2 eV, and 532.1 eV. The peaks at 528.9 eV and 530.2 eV are ascribed to oxygen in Ag_3PO_4 and TiO_2 lattices, respectively. The peaks at 532.1 eV indicate hydroxyls or the oxygen adsorbed on the surface of TiO_2/Ag_3PO_4. The results of XPS analysis further prove that Ag_3PO_4 and TiO_2 have been compounded.

The UV-Vis diffuse reflectance absorption spectra of the catalysts of $TiO_2$400, Ag_3PO_4, and $TiO_2$400/Ag_3PO_4 are

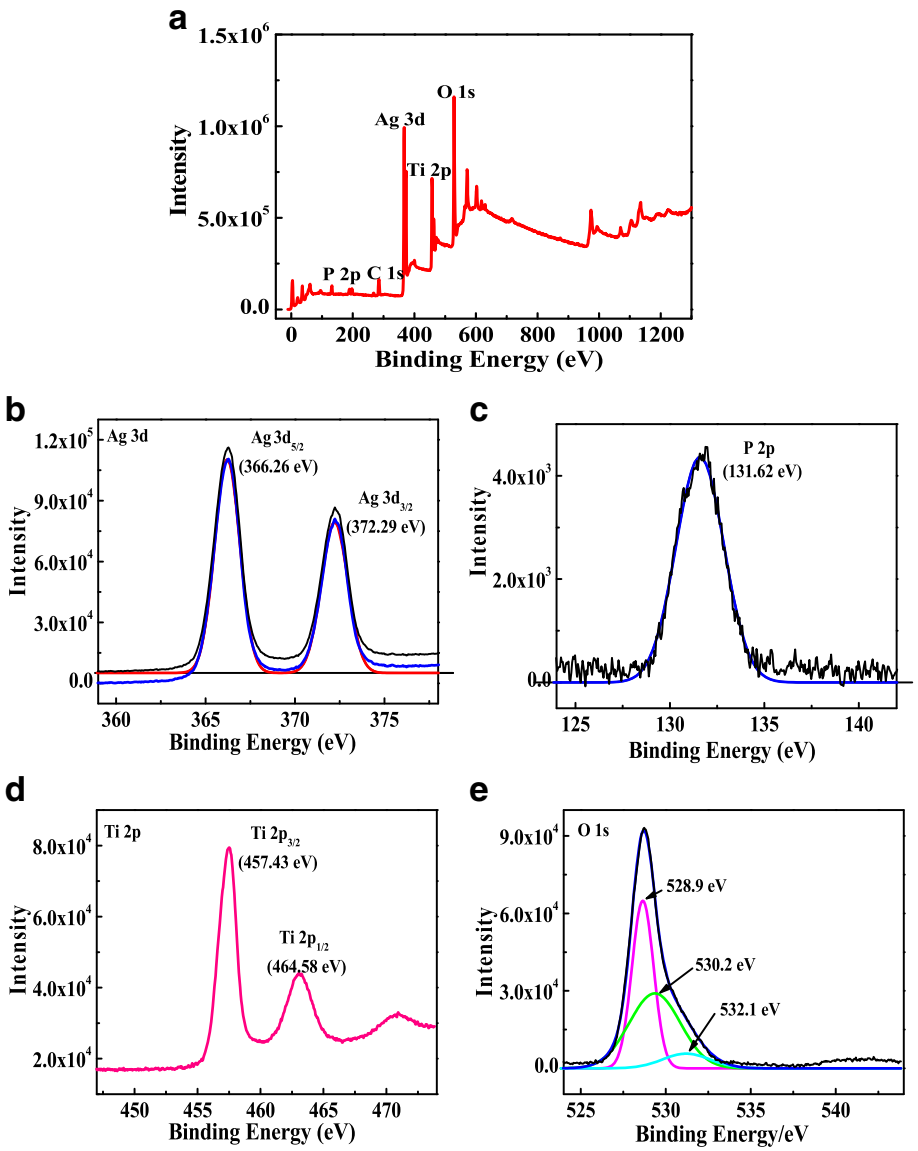

Fig. 3 XPS spectrum of $TiO_2$400/Ag_3PO_4: **a** survery scan, **b** Ag 3d, **c** P 2p, **d** Ti 2p, and **e** O1s

exhibited in Fig. 4a. It can be seen from the figure that the optical absorption cutoff wavelengths of $TiO_2$400 and Ag_3PO_4 are 400 and 500 nm, respectively. When Ag_3PO_4 is loaded on $TiO_2$400, the light absorption range of the composite obviously broadens to 500–700 nm, indicating that there is interaction between Ag_3PO_4 and $TiO_2$400 in the composite system of $TiO_2$400/Ag_3PO_4, and the mechanism needs further study. Bandwidth of Ag_3PO_4, $TiO_2$400, and $TiO_2$400/Ag_3PO_4 catalysts is computed with the Kubelka-Munk formula [17]:

$$Ahv = c(hv–Eg)^n$$

where A, hv, c, and Eg are the absorption coefficient, incident photon energy, absorption constant, and band gap energy, respectively. The value of n for direct semiconductor is 1/2, and that for indirect semiconductor is 2. Anatase TiO_2 and Ag_3PO_4 are indirect semiconductors, so n takes 2.

The plots depicting $(\alpha hv)^{1/2}$ versus incident photon energy (hv) from Fig. 4b indicates the band gap energy diagrams (Eg) of Ag_3PO_4, $TiO_2$400, and $TiO_2$400/Ag_3PO_4 catalysts are 2.45 eV, 3.1 eV, and 2.75 eV, respectively. This further proves that $TiO_2$400/Ag_3PO_4 is a good visible-light photocatalyst with suitable band gap width and visible light capture ability.

Photocatalytic degradation of RhB by $TiO_2$400, Ag_3PO_4, $TiO_2$300/Ag_3PO_4, $TiO_2$400/Ag_3PO_4, and $TiO_2$500/Ag_3PO_4 was investigated in Fig. 5a. The results showed that pure $TiO_2$400 had the worst photocatalytic effect, and the photocatalytic degradation rate was only 30% within 25 min. The photocatalytic degradation efficiency of pure Ag_3PO_4 was 69% after 25 min of irradiation. The photocatalytic degradation rate of $TiO_2$300/Ag_3PO_4 reached 40% after 25 min. The photocatalytic degradation rate of $TiO_2$500/Ag_3PO_4 was 80% after 25 min of irradiation. The best photocatalytic activity was $TiO_2$400/Ag_3PO_4, and 100% of RhB was decomposed after 25 min of illumination.

Figure 5b studied the kinetics model of photocatalytic degradation of RhB. From the figure, the photodegradation of RhB was followed pseudo-first-order kinetics and the reaction rate constant (k) was calculated with the slope of fitting curves. The reaction rate constant (k) values of each sample were shown in Table 1. The reaction rate constants of $TiO_2$400, Ag_3PO_4, $TiO_2$300/Ag_3PO_4, $TiO_2$400/Ag_3PO_4, and $TiO_2$500/Ag_3PO_4 were 0.00345 min^{-1}, 0.01148 min^{-1}, 0.00525 min^{-1}, 0.02286 min^{-1}, and 0.01513 min^{-1}, respectively. The sample $TiO_2$400/Ag_3PO_4 has the largest reaction rate constant, which is 0.02286 min^{-1}, twice that of Ag_3PO_4 and 6.6 times that of the minimum value of $TiO_2$400. This indicates that the combination of Ag_3PO_4 and TiO_2 can greatly contribute to the improvement of Ag_3PO_4 photocatalytic activity.

Figure 5c is the stability test result of four times of degradation of RhB solution by recycling of $TiO_2$400/Ag_3PO_4. The degradation effect of $TiO_2$400/Ag_3PO_4 shows good stability in four times of recycling, and in the fourth cycle experiment, the degradation effect of $TiO_2$400/Ag_3PO_4 was slightly higher than that of the third cycle. This may be due to the formation of composite material between Ag_3PO_4 and TiO_2 to accelerate photogenerated electron-hole pair transfer and in situ formation of a small amount of Ag in Ag_3PO_4 during photocatalysis to inhibit further photo-corrosion.

The results of TiO_2/Ag_3PO_4 capture factors are shown in Fig. 5d. After the addition of trapping agent IPA, the degradation activity decreased partially. When BQ and TEOA were added, the degradation degree of RhB decreased significantly, even close to 0. Therefore, we can infer that the main factors are holes (h^+) and superoxide anions (O·− 2), while hydroxyl radical (·OH) plays partially degradation.

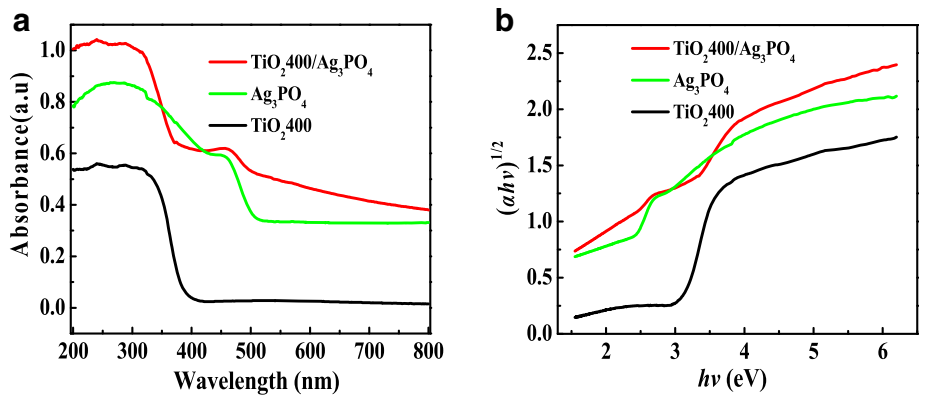

Fig. 4 $TiO_2$400, Ag_3PO_4, and $TiO_2$400/Ag_3PO_4 catalysts: **a** UV-Vis DRS, **b** plots of $(ahv)^{1/2}$ versus energy (hv)

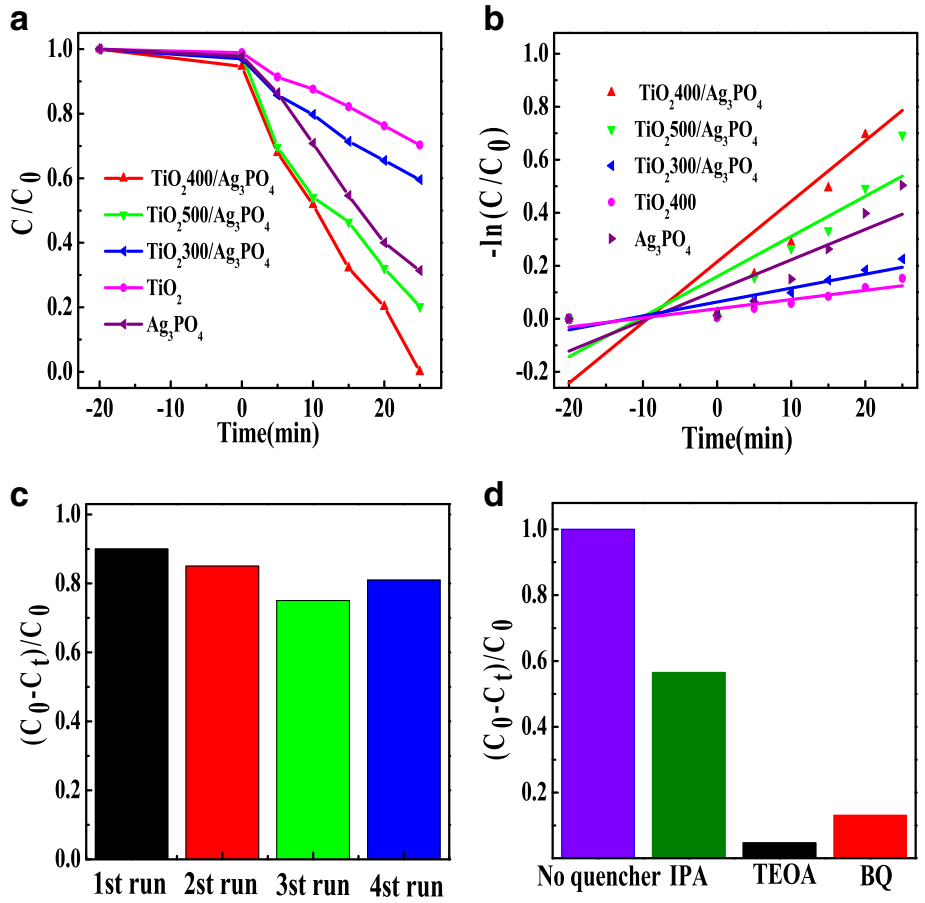

Fig. 5 **a** Effects of different catalysts on photocatalytic degradation of RhB under visible light. **b** First order kinetic fitting plots of photocatalytic degradation of RhB with different catalysts. **c** Cycling runs of TiO_2400/Ag_3PO_4. **d** Trapping experiments of active species

A possible Z-scheme photocatalytic degradation mechanism was proposed in Scheme 1 to expatiate the photocatalytic degradation of RhB by TiO_2/Ag_3PO_4 based on free radical capture and photodegradation experiments. The band gap of Ag_3PO_4 is 2.45 eV, and its E_{CB} and E_{VB} potential are ca.0.45 eV and 2.9 eV (vs. NHE) [18], respectively. As shown in Scheme 1, under visible light irradiation, Ag_3PO_4 is stimulated by photons with energy greater than its band gap to produce photogenerated electron-hole pairs. The holes left in the valence band of Ag_3PO_4 migrated to the valence band of TiO_2 and then directly participated in the RhB oxidation and decomposition process, which adsorbed on the surface of TiO_2. At the same time, during the migration of photogenerated holes, the H_2O and OH^- adsorbed on the composite surface can also be oxidized to form ·OH, and the highly oxidizing ·OH can further oxidize and degrade pollutants. This is mainly due to the energy of holes in the valence band of Ag_3PO_4 which is 2.9 eV, higher than the reaction potential energy of OH^-/OH ($E(OH^-/OH) = 1.99$ eV (vs. NHE)). However, the conduction potential of Ag_3PO_4 is 0.45 eV, the energy of photogenerated electrons is 0.45 eV, and the activation energy of single electron oxygen is $E(O_2/O\cdot-\ 2) = 0.13$ eV (vs. NHE). The photogenerated electrons on Ag_3PO_4 conduction band cannot be captured by dissolved oxygen. With the accumulation of photogenerated electrons on Ag_3PO_4 conductive band, a small amount of Ag nanoparticles has been formed due to the photocatalytic corrosion of Ag_3PO_4 photocatalyst. The formed Ag nanoparticles can also be stimulated by light energy to form photogenerated electron-hole pairs.

Table 1 Photo degradation rate constants and linear regression coefficients of different catalysts from equation $-\ln(C/C_0) = kt$.

	K (min^{-1})	Regression equation	R^2
TiO_2400/Ag_3PO_4	0.02286	$-\ln(C/C_0) = 0.02286x + 0.21496$	$R^2 = 0.68755$
TiO_2500/Ag_3PO_4	0.01513	$-\ln(C/C_0) = 0.01513x + 0.15984$	$R^2 = 0.753$
Ag_3PO_4	0.01148	$-\ln(C/C_0) = 0.01148x + 0.1079$	$R^2 = 0.71128$
TiO_2300/Ag_3PO_4	0.00525	$-\ln(C/C_0) = 0.00525x + 0.06354$	$R^2 = 0.82635$
TiO_2400	0.00345	$-\ln(C/C_0) = 0.00345x + 0.0383$	$R^2 = 0.78461$

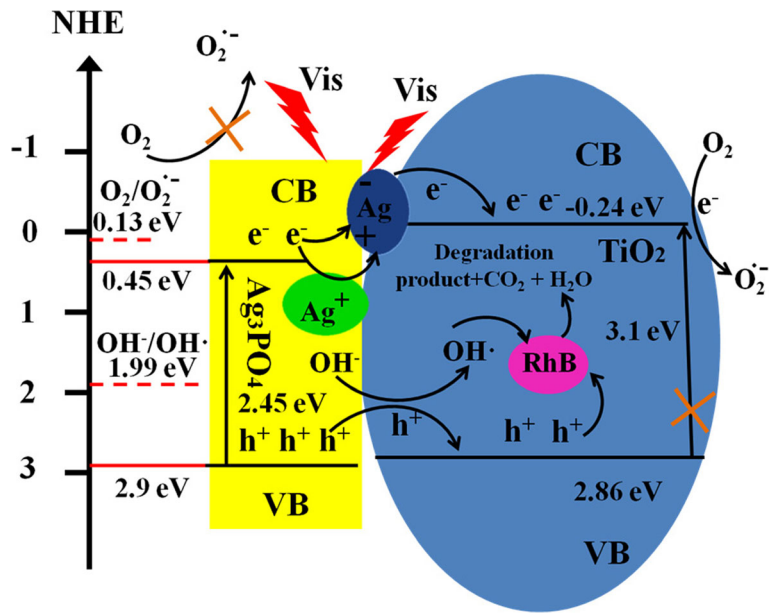

Scheme 1 Schematic illustration of the photocatalytic mechanism of TiO_2/Ag_3PO_4

Then the electrons migrated to the conduction band of TiO_2, while the holes left on the Ag nanoparticles can be compounded with the photogenerated electrons generated on the conduction band of Ag_3PO_4, thus preventing the further corrosion of Ag_3PO_4 photocatalyst. Due to the forbidden band of TiO_2 is 3.1 eV, it cannot be excited under visible light and the E_{CB} and E_{VB} are ca. − 0.24 eV and 2.86 eV (vs. NHE), respectively. Electrons injected into TiO_2 conduction band can degrade pollutants through trapping the oxygen adsorbed onto the TiO_2 surface. This is mainly due to the E_{CB} = − 0.24 eV (vs. NHE) which is more negative than E(O_2/O·- 2) = 0.13 eV (vs. NHE). The results are in accordance with the trapping experiments. The main factors are holes (h^+) and superoxide anions (O·- 2), while hydroxyl radical (·OH) plays partially degradation.

Basing on the above discussion, the degradation reaction of TiO_2/Ag_3PO_4 is expressed by the chemical equation as follows:

Generation of photoelectron hole pairs:

$$Ag_3PO_4 + hv \rightarrow Ag_3PO_4(e^-) + Ag_3PO_4(h^+)$$

$$Ag^+ + Ag_3PO_4(e^-) \rightarrow Ag + Ag_3PO_4$$

$$Ag + hv \rightarrow Ag(e^-) + Ag(h^+)$$

Migration and transformation of photogenerated hole electron pairs:

$$Ag_3PO_4(h^+) + TiO_2 \rightarrow TiO_2(h^+) + Ag_3PO_4$$

$$Ag_3PO_4(e^-) + Ag(h^+) \rightarrow Ag + Ag_3PO_4$$

$$Ag(e^-) + TiO_2 \rightarrow TiO_2(e^-) + Ag$$

$$TiO_2(e^-) + O_2 \rightarrow O_2^{\cdot-} + TiO_2$$

$$Ag_3PO_4(h^+) + 0H^- \rightarrow OH\cdot + Ag_3PO_4$$

Degradation of pollutants:

$$TiO_2(h^+) + RhB \rightarrow \text{Degradation product} + CO_2 + H_2O$$

$$O_2^{\cdot-} + RhB \rightarrow \text{Degradation product} + CO_2 + H_2O$$

$$OH\cdot + RhB \rightarrow \text{Degradation product} + CO_2 + H_2O + Cl^-$$

Conclusions

In summary, a comprehensive investigation of the composite Ag_3PO_4/TiO_2 photocatalyst, prepared by a simple two-step method is presented. Complementary characterization tools such as X-ray diffraction (XRD), scanning electron microscopy (SEM), transmission electron microscopy (TEM), high-resolution transmission electron microscopy (HR-TEM), energy dispersive X-ray spectroscopy (EDX), X-ray photoelectron spectroscopy (XPS), and UV-vis diffuse reflectance spectroscopy (DRS) were utilized in this study. The results showed that the composite Ag_3PO_4/TiO_2 photocatalyst is highly crystalline and has good morphology. For Ag_3PO_4/TiO_2 degradation of RhB, $TiO_2$400/Ag_3PO_4 shows the highest photocatalytic activity. After 25 min of reaction, the photocatalytic degradation rate reached

almost 100%. The reaction rate constant of $TiO_2$400/Ag_3PO_4 is 0.02286 min^{-1}, which is twice that of Ag_3PO_4 and 6.6 times that of the minimum value of $TiO_2$400. The $TiO_2$400/Ag_3PO_4 also exhibits good stability after recycling four times. The main active catalytic species are holes (h^+) and superoxide anions (O·– 2), while hydroxyl radical (·OH) plays partially degradation from trapping experiments. In addition, a Z-scheme reaction mechanism of Ag_3PO_4/TiO_2 heterogeneous structure is proposed to explain the RhB degradation mechanism. The accumulation of photogenerated electrons on Ag_3PO_4 conductive band causes photo-etching of Ag_3PO_4 photocatalyst to form a small amount of Ag nanoparticles, consequently, accelerating photogenerated electron transfer in the Ag_3PO_4 conduction band, thus preventing further Ag_3PO_4 photocatalyst corrosion.

Abbreviations

BQ: *p*-benzoquinone; DRS: UV-vis diffuse reflectance spectroscopy; EDX: Energy dispersive X-ray spectrometer; HR-TEM: High-resolution transmission electron microscopy; IPA: Isopropanol; RhB: Rhodamine B; SEM: Scanning electron microscopy; TEM: Transmission electron microscopy; TEOA: Triethanolamine; XPS: X-ray photoelectron spectroscopy; XRD: X-ray diffraction

Acknowledgements

This work is greatly indebted to professors Shuangqi Hu for his meticulous instruction and Lishuang Hu who helped us with great encouragement.

Authors' Contributions

This work presented here was performed in collaboration of all the authors. All authors read and approved the final manuscript.

Funding

No funding support.

Availability of Data and Materials

The authors declare that materials and date are promptly available to readers without undue qualifications in material transfer agreements. All data generated in this study are included in this article.

Competing Interests

The authors declare that they have no competing interests.

Received: 17 April 2019 Accepted: 4 June 2019
Published online: 13 June 2019

References

1. Li X, Fang S, Lei G, Han C, Ping Q, Liu W (2015) Synthesis of flower-like Ag/AgCl-Bi2MoO6 plasmonic photocatalysts with enhanced visible-light photocatalytic performance. Appl Catal B Environ:176, 62–177, 69
2. Yao W, Bo Z, Huang C, Chao M, Song X, Xu Q (2012) Synthesis and characterization of high efficiency and stable Ag3PO4/TiO2 visible light photocatalyst for the degradation of methylene blue and rhodamine B solutions. J Mater Chem 22:4050
3. Fujishima A, Honda K (1972) Electrochemical Photolysis of Water at a Semiconductor Electrode. Nature 238:37–38
4. O'Regan B, Grätzel M, Fitzmaurice D (1991) Optical electrochemistry I: steady-state spectroscopy of conduction-band electrons in a metal oxide semiconductor electrode. Chem Phys Lett 183:89–93
5. Li Z, Yu J, Fan J, Zhai P, Wang S (2009) Dye-sensitized solar cells based on ordered titanate nanotube films fabricated by electrophoretic deposition method. Electrochem Commun 11:2052–2055
6. Shan Z, Wu J, Xu F, Huang FQ, Ding H (2008) Highly Effective Silver/Semiconductor Photocatalytic Composites Prepared by a Silver Mirror Reaction. J Phys Chem. C 112:15423–15428
7. Xiaobo C, Lei L, Yu PY, Mao SS (2011) Increasing Solar Absorption for Photocatalysis with Black Hydrogenated Titanium Dioxide Nanocrystals. Science 331:746–750
8. Livraghi S, Votta A, Paganini MC, Giamello E (2005) The nature of paramagnetic species in nitrogen doped TiO2 active in visible light photocatalysis. Chem Commun 4:498–500
9. Yu L, Yu H, Mei C, Sun J (2012) Microwave hydrothermal synthesis of Ag2CrO4 photocatalyst for fast degradation of PCP-Na under visible light irradiation. Catal Commun 26:63–67
10. Wang X, Li S, Yu H, Yu J, Liu S (2011) Ag2O as a New Visible-Light Photocatalyst: Self-Stability and High Photocatalytic Activity. Chemistry 17: 7777–7780
11. Lee S, Park Y, Pradhan D, Sohn Y (2016) AgX (X = Cl, Br, I)/BiOX nanoplates and microspheres for pure and mixed (methyl orange, rhodamine B and methylene blue) dyes. J Ind Eng Chem 35:231–252
12. Zhiguo Y, Jinhua Y, Naoki K, Tetsuya K, Shuxin O, Hilary SW, Hui Y, Junyu C, Wenjun L, Zhaosheng L (2010) An orthophosphate semiconductor with photooxidation properties under visible-light irradiation. Nat Mater 9:559–564
13. Yao W, Fang X, Guo D, Gao Z, Wu D, Kai J (2013) Synthesis of ZnO/CdSe hierarchical heterostructure with improved visible photocatalytic efficiency. Appl Surf Sci 274:39–44
14. Peng Y, Yan M, Chen QG, Fan CM, Zhou HY, Xu AW (2014) Novel one-dimensional Bi2O3–Bi2WO6 p–n hierarchical heterojunction with enhanced photocatalytic activity. J Mat Chem A 2:8517–8524
15. Li J, Guo Z, Yu W, Zhu Z (2014) Three-dimensional TiO2 /Bi2WO6 hierarchical heterostructure with enhanced visible photocatalytic activity. Micro Nano Lett let 9:65–68
16. Zheng C, Hua Y (2018) Assembly of Ag3PO4 nanoparticles on rose flower-like Bi2WO6 hierarchical architectures for achieving high photocatalytic performance. J Mater Sci Mat Electron 29:9291–9300
17. Schuhl Y, Baussart H, Delobel R, Bras ML, Leroy JM, Gengembre L, Grimblot J (1983) Study of mixed-oxide catalysts containing bismuth, vanadium and antimony. Preparation, phase composition, spectroscopic characterization and catalytic oxidation of propene. Chem Inf 14:2055–2069
18. An Y, Zheng P, Ma X (2019) Preparation and visible-light photocatalytic properties of the floating hollow glass microspheres – TiO2/Ag3PO4 composites. RSC Advances

Publisher's Note